Adaptive Multiphoton Endomicroscope Incorporating a Polarization-Maintaining Multicore Optical Fibre

Youngchan Kim, Sean C. Warren, James M. Stone, Jonathan C. Knight, Mark A. A. Neil, Carl Paterson, Chris W. Dunsby, and Paul M. W. French

***Abstract*—We present a laser scanning multiphoton endomicroscope with no distal optics or mechanical components that incorporates a polarization-maintaining (PM) multicore optical fibre to deliver, focus, and scan ultrashort pulsed radiation for two-photon excited fluorescence imaging. We show theoretically that the use of a PM multicore fibre in our experimental configuration enhances the fluorescence excitation intensity achieved in the focal spot compared to a non-PM optical fibre with the same geometry and confirm this by computer simulations based on numerical wavefront propagation. In our experimental system, a spatial light modulator (SLM) is utilised to program the phase of the light input to each of the cores of the endoscope fibre such that the radiation emerging from the distal end of the fibre interferes to provide the focused scanning excitation beam. We demonstrate that the SLM can enable dynamic phase correction of path-length variations across the multicore optical fibre whilst the fibre is perturbed with an update rate of 100 Hz.**

***Index Terms*—Adaptive optics, multiphoton endomicroscope, polarization-maintaining multicore optical fibre, and wavefront shaping.**

I. Introduction

MULTIPHOTON microscopy [1] provides inherently optically sectioned images, enabling biochemical structure and activity to be studied in biological tissue [2]–[4], and is increasingly applied in vivo. To explore its potential for preclinical and clinical imaging, several groups are developing miniaturized instruments for multiphoton endomicroscopic imaging [5]–[14]. Most commonly these approaches are based on miniaturization of distal scanning and optical components integrated with a fibre-optic delivery system that can be implemented using double-clad large mode area photonic crystal fibre [15] or hollow-core photonic crystal fibre for minimal dispersion [16] with the double-cladding providing a high epi-detection efficiency through the inner cladding. To reduce the minimum size of endoscopes beyond the limits imposed by the size of the distal components, it is interesting to consider approaches that require no distal scanner. One such approach is proximal scanning of the excitation beam focused at the proximal end of a multicore optical fibre to sequentially couple into the individual cores. Thus transverse scanning is realised at the distal end with no need for mechanical components [17], although distal optics are required for focusing light into the sample and these must be translated to adjust the position of the focal plane. This approach is in clinical use [5] and has been adapted for rapid fluorescence lifetime imaging, including for FRET experiments [6]. We have previously presented [18] a further approach to laser scanning endomicroscopy that enables 3-D imaging without any distal mechanics or optics, utilising a multicore optical fibre in which multiple cores are simultaneously illuminated. At the distal end of the multicore fibre, the phase of the radiation emerging from each of the multiple fibre cores is controlled so as to interfere to produce a focused scanning beam in a manner analogous to phased-array radar. This is realised using a spatial light modulator (SLM) at the proximal end of the multicore optical fibre to precompensate for aberrations arising from differences in the pathlengths of the fibre cores and to control the phase profile of the light at its output. This approach could ultimately permit the production of thinner endomicroscopes and also facilitate coherent imaging and adaptive aberration correction. For multiphoton endoscopy, this approach enables the transmission of the excitation radiation with significantly lower peak intensity per core compared to propagating ultrashort pulses in a single mode optical fibre (or a single fibre core), thereby reducing nonlinear optical effects that can lead to pulse broadening and/or distortion. In subsequent work it has been implemented with a double-clad multicore optical fibre to realise a lensless multiphoton endoscope [19].

This proximal phase-correction approach is similar in concept to the adaptive optics techniques used for the control of beam propagation through inhomogeneous media that have been studied in the context of atmospheric propagation [20] and more recently used in optical microscopy [21]–[23]. Several groups have extended this to transmit images through a single multimode optical fibre, utilising the higher order modes to convey the image information [24]–[26]. While this approach is compact and does not require specialised multicore optical fibres, the modal dispersion makes it challenging to transmit the ultrashort pulses required for multiphoton excitation, although we note progress is being made in this area by restricting the modes utilised to a small subset with similar optical path lengths [27].

Manuscript received May 28, 2015; revised August 7, 2015; accepted September 29, 2015. Date of publication October 7, 2015; date of current version November 10, 2015. This work was supported by a UK Engineering and Physical Sciences Research Council Healthcare Technologies Challenges for Engineering research under Grant (EP/K020102/1). Y. Kim and S. C. Warren contributed equally to this work.

Y. Kim, S. C. Warren, M. A. A. Neil, C. Paterson, and P. M. W. French are with the Photonics Group, Department of Physics, Imperial College London, London SW7 2AZ, U.K. (e-mail: youngchan.kim@imperial.ac.uk; sean.warren09@imperial.ac.uk; mark.neil@imperial.ac.uk; carl@imperial.ac.uk; paul.french@imperial.ac.uk).

C. W. Dunsby is with the Centre for Histopathology, Imperial College London, London W12 0NN, U.K. (e-mail: christopher.dunsby@imperial.ac.uk).

J. M. Stone and J. C. Knight are with the Centre for Photonics and Photonic Materials, Department of Physics, University of Bath, Bath BA2 7AY, U.K. (e-mail: py1jms@bath.ac.uk; pysjck@bath.ac.uk).

Color versions of one or more of the figures in this paper are available online at http://ieeexplore.ieee.org.

Digital Object Identifier 10.1109/JSTQE.2015.2488283

In our previous work [18], we utilised a single interferogram recorded at the distal end of the fibre bundle to determine the phase required at the input of all of the fibre cores in order to correct for path length variations between them. While this offered the relative advantage of simplicity over the methods used in other work [19], [27], [28] that required separate distal interferometric measurements to determine the required phase for the input of each fibre core (or mode), our implementation of the algorithm required many seconds to calculate the required phase distribution and to apply it to the SLM, which is not practical for endoscopy. In this paper, we report progress towards the development of an ultracompact laser scanning multiphoton endomicroscope with no distal optics or mechanical components and demonstrate real-time dynamic correction of the required input phases at the proximal end of the multicore optical fibre with an update rate of 100 Hz. We further demonstrate the use of a novel polarization-maintaining multicore optical fibre [29] that increases the efficiency and contrast of the system without the need for a distal polarization filter.

II. Methods

A. Double-Clad Polarization-Maintaining Multicore Fibre

We used a novel double-clad polarization-maintaining (PM) multicore fibre with 98 cores and low cross-talk [29] that was designed to achieve single mode operation at a wavelength of 800 nm with the cores arranged in a rectangular structure with center-to-center distances of 14 and 16 μm in the horizontal (x) and vertical (y) directions (relative to the image shown in the inset of Fig. 1(a)). Each core was manufactured from a gradient index germanium doped silica preform (Draka–Prysmian) with a pure silica jacket. The numerical aperture (NA) of the preform was 0.3 and the final core diameter in the fibre was 2 μm. To preserve the polarization of input light, stress-applying rods manufactured from boron doped silica (Draka–Prysmian) were inserted into the fibre—identifiable as the dark features in the inset of Fig. 1(a). The overall diameter of the 98 cores and inner cladding was 230 μm. To improve the signal collection efficiency in the PM fibre necessary for proximal detection, the inner cladding was jacketed with a fluorine doped low refractive index outer cladding material (Heraeus), providing multimode guiding for fluorescence collection with a NA $= 0.2$. Thus the outer diameter of the whole double-clad PM multicore fibre was 260 μm.

B. Experimental Setup

The experimental set-up for the adaptive multiphoton endomicroscope is illustrated in Fig. 1(a). Excitation pulses of 100 fs duration were provided by a Ti:Sapphire mode-locked femtosecond laser (Tsunami 3941-M3BB, Spectra-Physics) at 800 nm centre wavelength and 80 MHz repetition rate with 10.9 nm spectral bandwidth and a corresponding coherence length of 52 μm. For the low average power ($\sim$1 mW) in each optical fibre core used here, there was no measureable increase in spectral bandwidth after propagation through the PM multicore fibre. Thus we expect negligible pulse broadening due to

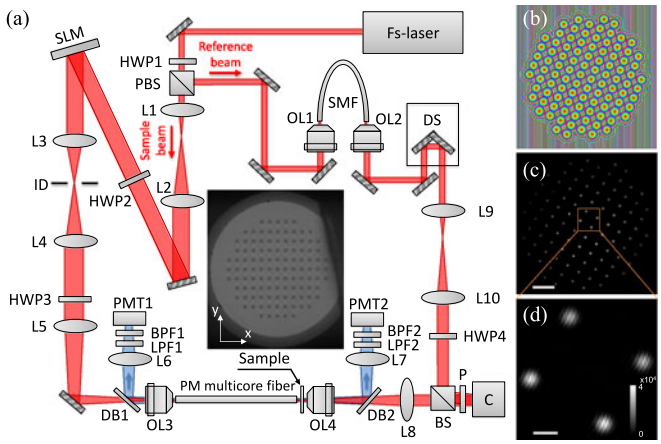

Fig. 1. (a) Schematic diagram of the experimental setup. HWP1–4, half-wave plates; PBS, polarizing beam splitter; L1–10, lenses ($f = 50$, 300, 100, 150, 200, 100, 100, 150, 50, and 300 mm, respectively); SLM, spatial light modulator; PM multicore fibre, polarization-maintaining multicore fibre; SMF, single mode fibre, ID, iris diaphragm; PMT1-2, photomultiplier tubes; BPF1-2, band-pass filters; DB1-2, dichroic beamsplitters, filters LPF1-2, low-pass filters; OL1-4, microscopic objectives (10×, 10×, 40×, and 20×, respectively); DS, delay stage; BS, beam splitter; P, polarizer; C; camera. Red and blue arrows correspond to the direction of fs laser and two-photon excited fluorescence light respectively. The length of the PM multicore fibre was 30 cm. Inset shows an optical micrograph of the PM multicore fibre. (b) Example of phase map applied on the SLM. The color map represents phases, ranging from 0 to 2π. (c) Example of interferogram for the distal end of the multicore fibre. Scale bar 30 μm. For clarity, the image of the reference beam was subtracted from the image of raw interferogram. (d) A zoomed-in region of (c). Scale bar 5 μm.

self-phase modulation and can calculate that the pulses will be broadened by the group velocity dispersion (GVD), which is dominated by the material dispersion at 800 nm, to result in an output pulse duration of 370 fs after propagation through the 30 cm long PM multicore fibre. We measured the optical path length variation between cores of the PM multicore fibre and found that the standard deviation was 31.9 μm, which is less than the coherence length.

The laser beam was split into two arms of a Mach–Zehnder interferometer via a polarizing beam splitter (PBS), one part to be delivered to the sample via the multicore fibre and the other providing a reference beam enabling optical path length variations between cores to be measured from interference fringes recorded by the camera (C). The relative intensity between the two beams was controlled by rotating the half-wave plate (HWP1). In the sample arm, the beam incident on the SLM (HSPDM512, Boulder Nonlinear Systems) was expanded through a magnifying telescope (L1 and L2) and its polarization was rotated to be vertical by HWP2 in order for it to be aligned with the axis of the SLM. We used a phase-only reflection SLM, which has 512×512 pixels and a pixel pitch of 15 μm. As part of the alignment process, the SLM was initially imaged onto the proximal end of the multicore fibre with a de-magnification factor of $M = 30$ by two 4-f imaging systems (L3, L4 and L5, OL3). To minimize the intensity of light propagating through the cladding and to transmit the light through the cores of the multicore fibre efficiently, a microlens array of focal length $f = 36$ mm was generated on the SLM, as shown in Fig. 1(b). Subsequently the proximal end of the multicore fibre was translated 40 μm from

the focal plane of the proximal objective lens (OL3), i.e., by the focal length of the microlenses divided by the axial magnification (f/M^2). With the microlens spacing equal to the fibre core spacing this arrangement results in a light injection numerical aperture of approximately 0.19. Thus the SLM could be used to control the phase of the light coupled into each fibre core. To further minimise the amount of excitation light travelling in the cladding of the multicore fibre, binary amplitude modulation was implemented by applying a large phase-ramp to those areas of the SLM where an amplitude of zero was required. Such light diffracted from these regions was blocked by an iris diaphragm (ID) placed between L3 and L4. The distal end face of the multicore fibre was imaged onto a scientific complementary metal oxide semiconductor camera (Zyla 10-tap sCMOS, Andor) through a 4-*f* imaging system (OL4 and L8) with 16.7 magnification.

In principle, the phase modulation scheme above should be able to provide phase-only modulation without affecting the coupling efficiency into the multicore fibre. In practice, however, the power transmitted through each core with the phase correction applied relative to the power transmitted with no phase correction applied was 1.03 ± 0.19 (mean $\pm$ standard deviation over all cores), which could be attributed to the wrapping of the microlens phase profile due to the limited phase-stroke of the SLM and/or to a misalignment of the polarization state of the beam incident on the SLM relative to the vertical axis of the SLM.

For the initial calibration, the sample shown in Fig. 1(a) was not present. In the reference arm of the interferometer, a single mode fibre (780 HP, Thorlabs) of the same length (30 cm) as the PM multicore fibre was used to approximately match the dispersion in the two arms. The sample and reference beams were recombined to generate interference fringes on the camera using a non-polarizing beamsplitter (BS). A polarizer (P) placed in front of the camera was used during alignment of HWP3 to ensure that light in the sample arm was correctly coupled into one axis of the PM multicore fibre. HWP4 was used to rotate the orientation of the reference beam polarization state to match that from the distal end of the fibre so as to maximize the contrast of interference fringes obtained. The relative time delay between the sample and the reference beams was adjusted to maximize the contrast of the interference fringes using the mechanical delay stage (DS). Fig. 1(c) shows an image of the interferogram. The reference arm beam was aligned so as to produce a fringe pattern with a period of 14 μm at the location of each fibre core, as shown in Fig. 1(d). Thus we could measure an interferogram associated with phase distribution at the distal end of the multicore fibre. The system was controlled through a custom-written software package written in C++.

In order to determine the affine transformation between the SLM pixels and the camera pixels, we displayed 5 well-separated microlenses on the SLM. In the first alignment step, their positions were adjusted manually so that the light was coupled through five separate cores of the fibre. A software algorithm was then applied to optimize the position of each of the five microlenses individually to maximize the coupling through each core. The positions of these five conjugate positions were used to calculate the affine transformation from SLM to camera coordinates [30]. We were then able to calculate the corresponding SLM coordinates for each fibre core image on the camera.

To correct the phase distortion introduced by the variation in pathlength of individual cores and achieve 3-D scanning of a focused beam at the distal end of the multicore fibre, we conducted the following procedures:

1) The phase of the optical field exiting each core of the multicore fibre was calculated from the interferogram acquired on the camera using a Fourier-transform method [31].
2) For each core on the interferogram, the corresponding SLM microlens was identified using the affine transformation from SLM to camera coordinates.
3) The phase of each microlens at the SLM is adjusted to eliminate the phase variation between cores that was measured in step 1.
4) Subsequently the SLM is programmed to impose appropriate phase curvature on the light emerging from the fibre cores in order to form a focused beam spot and to realize 3-D scanning at the distal end of the multicore fibre as described in reference [18].

To demonstrate two-photon excited fluorescence (TPEF) imaging, a sample was inserted at the focal plane of the wavefronts emerging from at the distal end of the multicore fibre. TPEF from the sample was transmitted by the multimode inner cladding of the multicore fibre for proximal detection by PMT1 (PMH-100-0, Becker & Hickl GmbH) after the dichroic beamsplitter DS1 (Di01-R594-25×36, Semrock).

TPEF could also be collected in transmission by a microscope objective (OL4) and reflection from the dichroic beamsplitter DS2 (Di01-R594-25×36, Semrock) to be detected by the photomultiplier tubes PMT2 (PMH-100-0, Becker & Hickl GmbH), respectively. Band-pass (FF02-470/100-25, Semrock) and low-pass filters (FF01-680/SP-25, Semrock) located in front of the PMTs were used to block any residual light from the excitation laser.

III. Results

A. Phase Correction and Control

We measured the phase of the optical field of the radiation emerging from every core of the PM multicore fibre before and after phase correction, as shown in Fig. 2(a) and (b). The phases before correction (see Fig. 2(a) and (c)) are randomly distributed due to the phase distortions caused by the PM multicore fibre, whereas the corrected phase map and angular histogram after phase correction (see Fig. 2(b) and (d)) show a narrower distribution. The circular variances measured from the angular histograms before and after phase correction correspond to 0.849 and 0.011, respectively.

For practical endoscopy, it is essential to compensate for aberrations arising from variations in pathlength across the cores of the multicore optical fibre dynamically. To ensure stable phase control, a key step is to demonstrate real time phase stabilisation, which we implemented here by imaging the distal interferograms of the end face of the fibre at a frame rate of

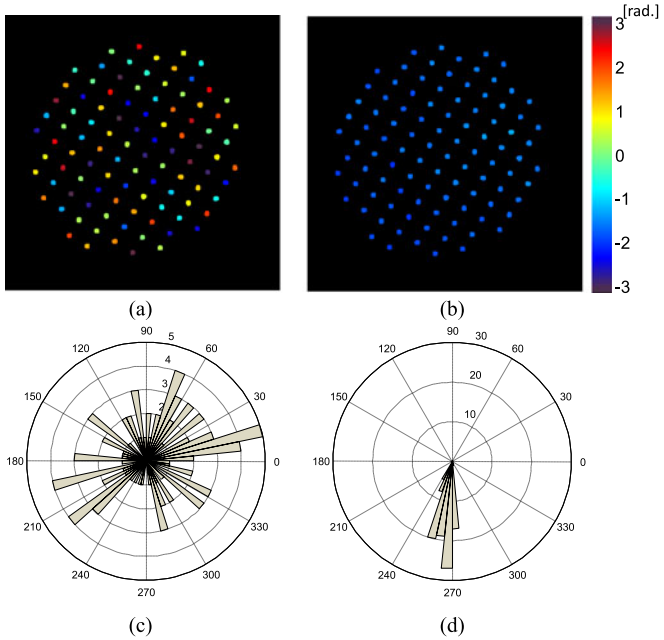

Fig. 2. Phase maps at the distal end of the PM multicore fibre and corresponding angular histograms in each case; (a) phase map before phase correction, (b) phase map after phase correction, (c) angular histogram before phase correction, and (d) angular histogram after phase correction. The radial scale on the histograms represents the number of cores whose phase values fall within each histogram bin and the phase angle of each bin is displayed in degrees on the outer circumferential scale. In (c) and (d) the maximum radial scales represent 5 and 30 cores, respectively. In (a) and (b) the phase measured at each core is represented by the color of a circle centered on each core's location. Gaps between cores are colored black.

417 Hz using a sCMOS camera (Zyla 10-tap sCMOS, Andor). The phase at each core was determined using the algorithm previously described [16] and a proportional-integral-derivative (PID) controller was implemented for each core to estimate the phase compensation to apply to the microlens array on the SLM. The interferogram processing, PID filter and microlens array calculation was implemented on a GPU (Nvidia GeForce GTX960). The phase compensation calculation required 1.5 ms in total to execute for the 512×512 pixel camera image and dynamic phase correction of every core of the fibre was realised with an update rate of 100 Hz determined by the switching rate of the SLM liquid crystals.

Fig. 3 demonstrates the performance of the dynamic phase correction algorithm. A phase correction procedure utilising a single distal interferometric measurement was performed at the start of the experiment. Initially the sample was static with the dynamic phase correction switched off and the phase in every core was measured at 417 Hz. The mean value of the circular variance of the phase was 0.015 over the time period $t = 0 - 5.7$ s when the PM multicore fibre was stationary (i.e., with no perturbation applied). At $t = 5.7$ s, a 4 Hz sinusoidal voltage was applied to a loudspeaker cone to introduce $\sim 10°$ of bend to the PM multicore fibre at its midpoint along its length with a repetition rate of 4 Hz. This motion caused the mean value of the circular variance of the phase to increase to 0.221 for the time period $t = 5.7 - 11.5$ s. At $t = 11.5$ s we switched on the dynamic phase correction and the mean value of the circular

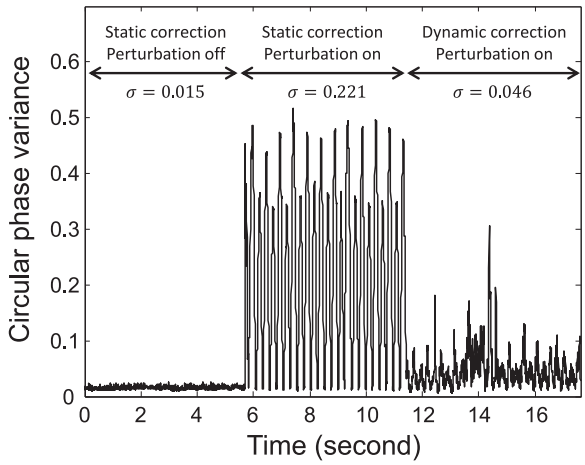

Fig. 3. Circular variance of the phase measured in every core of the PM multicore fibre whilst measuring and correcting the phase applied to each core at 100 Hz. Initially, the fibre was stationary. A mechanical sinusoidal perturbation to the fibre's pathlength distribution was started at time $t = 5.7$ s. At $t = 11.5$ s the algorithm applying dynamic phase correction was switched on.

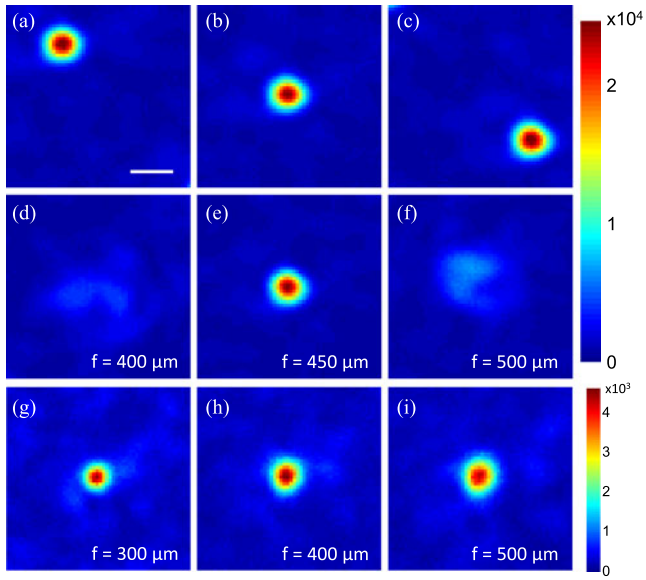

Fig. 4. Intensity images demonstrating 3-D scanning of the focused beam spot. (a)–(c) Examples of the beam spot focused to different lateral positions for an applied focal length of 450 μm. In (d)–(j), the applied focal length is indicated in each image. In (a)–(f), the images were acquired at a fixed observation plane located at 450 μm from the distal end of the PM multicore fibre, while the images in (g)–(j) were acquired at the focal plane applied. Scale bar 5 μm.

variance of the phase reduced to 0.046, illustrating the ability of the system to compensate for the applied motion in real time.

Fig. 4 illustrates how the phase control enables the focused spot to be scanned in three dimensions by varying the phase map applied to the SLM in order to adjust the tilt and curvature of the wavefronts emerging from the distal end of the multicore fibre. In Fig. 4(g)–(j) we illustrate the focal spot formed as we vary the focal length from 300 to 500 μm. As the focal length is increased the effective numerical aperture of the focused spot is decreased and so the full width at half maximum (FWHM) of the focused spot increases accordingly.

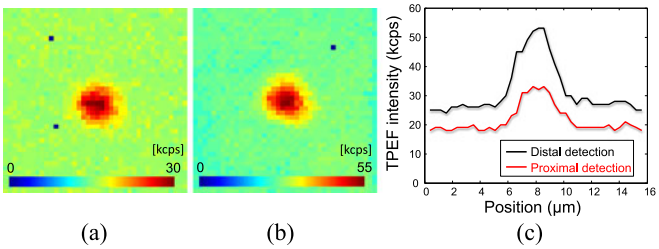

Fig. 5. Two-photon excited fluorescence images of a 2.16 μm fluorescence bead (Light Yellow, Spherotech, Inc.) using (a) the proximal and (b) the distal detection. (c) The line profiles along the horizontal axis across the maximum intensity in (a) and (b). The black dots corresponding to a value of zero in (a) and (b) were caused by a software artifact.

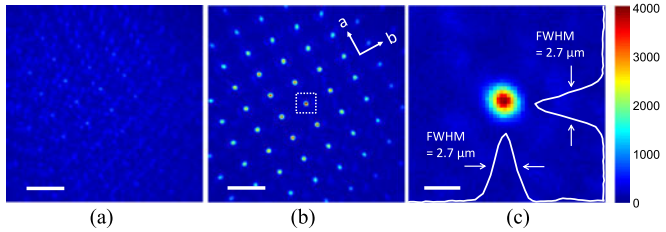

Fig. 6. Intensity images measured at the object plane 400 μm from the distal end of the PM multicore fibre (a) before and (b) after phase correction for an applied focal length of 400 μm. (c) The enlarged image of the dotted white square in (b). The solid lines in (c) represent the horizontal and vertical line profiles across the center of the focused beam spot. Scale bar in (a) and (b) 30 μm, scale bar in (c) 4 μm.

B. Two-Photon Excited Fluorescence Imaging

To verify the applicability of adaptive multiphoton endomicroscope for TPEF imaging, we acquired TPEF images of a single fluorescence bead with both proximal and distal detection, as shown in Fig. 5. The measurements were performed with an applied focal length of 450 μm. The fluorescence signal is lower for proximal detection due to the lower fluorescence collection NA provided by the inner-cladding of the multicore fibre (NA $= 0.2$) compared to the NA of the distal objective (OL4, NA $= 0.4$). The background signal in the TPEF images was attributed to two-photon excited autofluorescence generated from the multicore fibre itself. Using a higher input power to the fibre increases not only the peak power at the central focused spot but also the background autofluorescence by the same factor. This background autofluorescence could be decreased in the future by increasing the number of cores in the multicore fibre to reduce the excitation power in any single core: for example, increasing the number of cores by a factor of 10 should reduce the background signal by a factor of 100.

The data shown in Fig. 5(c) was fitted to a Gaussian function and the FWHM was measured as 2.8 μm. The diameter of the fluorescent bead (2.16 μm) can be accounted for approximately by assuming that both the point spread function and the bead are Gaussian functions and this yields an estimated two-photon lateral resolution of $\sqrt{2.84^2 - 2.16^2} \approx 1.8\,\mu\text{m}$.

C. Generation of Multiple Foci and Limitation of the Field of View

A consequence of the light emerging from the periodic arrangement of fibre cores is that the coherent interference results in a periodic array of foci, as illustrated in Fig. 6, which shows the intensity distributions measured 400 μm away from the distal end of the multicore fibre with the phase of the cores programmed to generate a focal length of 400 μm. Before phase correction, the intensity distribution at the focal plane is a speckle pattern caused by random interference of light emitted by each core at the distal end of the multicore fibre (see Fig. 6(a)). After the phase correction and application of the appropriate curved phase profile, multiple focused beam spots were observed, as can be seen in Fig. 6(b). Because the different foci are not independently controllable, the maximum size of object that can be imaged is limited by the separation distances between the central and the adjacent focused spots. For the applied focal length, these are 19 and 22 μm for the indicated axes *a* and *b*. Fig. 6(c) shows the central focused beam spot whose FWHM is 2.7 μm, which determines the lateral resolution when imaging with this system. The average power within the central spot was 374 μW.

For future work, both the peak power in the central focus and the separation between foci could be increased by designing a multicore fibre with smaller center-to-center separation of cores, such that fewer foci fall within the intensity envelope of the radiation emitted by the cores. Alternatively a single illumination focus could be achieved if the multicore fibre could be designed with a random spatial distribution of fibre cores.

D. Advantage of PM Multicore Fibre

The PM multicore fibre offers a significant increase in the intensity achieved in the focal spot compared with a non-PM fibre. This is because there is no depolarization of the light coupled into each core and therefore all of the light exiting each core the fibre can be programmed to have the correct phase to interfere to form the focal spot. In both cases, the field at the focal plane is the coherent superposition of the contributions from each fibre core. For the PM fibre, after phase correction, all components have the same magnitude, polarization and phase so the amplitude at focus A_{PM} after correction of the phase is the sum of the magnitudes *a* from each of *N* cores

$$A_{\text{PM}} = \sum_{i}^{N} a = Na. \tag{1}$$

In the case of the non-PM fibre, the polarization state emitted from each core is randomized, i.e., with a uniform probability density over the surface of the Poincaré sphere described by a normalized Stokes vector [1, Q, U, V] [32]. A single phase correction can only compensate for one of two independent polarization states: here we use horizontal linear but the choice is arbitrary. In this situation, by projecting the surface of Poincaré sphere onto the Q axis that describes the horizontal-vertical linear states, it can be shown that Q has a uniform probability density of $p(Q) = 1/2$ over the range $-1 \leq Q \leq 1$. Therefore, the intensity of the horizontal linear state I_H over the range $0 \leq I_H \leq 1$ given by

$$I_H = \frac{Q+1}{2} \tag{2}$$

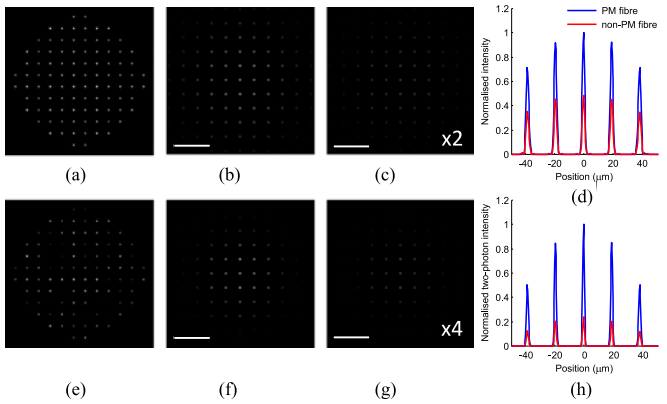

Fig. 7. Numerical simulations for generation and propagation of distal wavefronts at the distal end of PM and the non-PM multicore fibres. (a) and (e) The simulated intensity map in the horizontal polarization state of the distal end of both PM and non-PM multicore fibres. (b) and (c) show the calculated total intensity images for the PM and non-PM multicore fibres at the focal plane. (f) and (g) show the two-photon intensity distribution images for the PM and non-PM multicore fibres. (d) shows normalized horizontal line profiles across the center of intensity images for (b) the PM and (c) the non-PM muilticore fibres. (h) shows the corresponding normalized line profiles taken across the center of (f) and (g). For clarity, (c) intensity and (g) two-photon intensity images for the non-PM multicore fibre were displayed with $\times 2$ and $\times 4$ gains, respectively compared to (b) and (f). Scale bars 50 μm.

also has a uniform probability density with $p(I_H) = 1$. This gives a mean magnitude of the horizontal polarization component of

$$\langle |E_H| \rangle = \int_0^1 |E_H|\, p(I_H) \mathrm{d}I_H = \int_0^1 \sqrt{I_H} \mathrm{d}I_H = 2/3. \quad (3)$$

As with the PM fibre, the amplitude at the focus after phase correction is a sum of magnitudes from each core, but in this case the magnitudes only of the chosen polarization component. This gives

$$A_{\text{non-PM}} = \sum_i^N a \langle |E_H| \rangle = \frac{2}{3} N a. \quad (4)$$

This results in an increase in the achievable intensity at focus of $(3/2)^2$ and in the two-photon response of $(3/2)^4 \approx 5.1$ for the PM fibre compared to the non-PM fibre.

The above comparison assumes that the dispersion properties of the simulated PM and non-PM multicore fibres are identical. This is a reasonable assumption when working at 800 nm in silica glass because the excitation radiation is far from the zero GVD wavelength ($\sim$1.3 μm) and any differences in waveguide dispersion would be small compared to the material dispersion at 800 nm for both PM and non-PM multicore optical fibres.

To illustrate this, we numerically simulated the propagation of the wavefront from the distal end of multicore fibre to the focal plane using the angular spectrum method [33] implemented in MATLAB. The simulated cores were laid out on a rectangular grid as shown in Fig. 7(a). The coordinates of the jth core are notated (x_j, y_j). The field produced by each core was approximated by a circularly symmetrical Gaussian profile with mode field diameter r. For a non-PM multicore fibre, each core was assigned an amplitude of $\sqrt{I_H}$ for the horizontal component where I_H is drawn from a uniform distribution over the range 0 to 1. The amplitude of the vertical component was then $\sqrt{1 - I_H}$, together with a random phase shift δ_j as the phase of this polarization state is not corrected. A steering phase φ_j was applied to each core to form a focus at a distance of 400 μm [18]. In the case of a PM multicore fibre, the field from each core was assumed to have only the unit horizontal component. The components of the field corresponding to parallel and perpendicular with respect to the input polarization, $C_{jH}(x, y)$ and $C_{jV}(x, y)$ respectively, are shown in

$$\left.\begin{aligned} C_{jH}(x, y) &= \sqrt{I_H} \\ C_{jV}(x, y) &= \sqrt{1 - I_H} e^{i\delta_j} \end{aligned}\right\} \times e^{i\varphi_j} \sqrt{\frac{2}{\pi}} \frac{1}{\sigma} e^{\frac{(x-x_j)^2 + (y-y_j)^2}{\sigma^2}}. \quad (5)$$

In this simulation, the field at the end face of the fibre was given by the sum of the fields produced by each core. To calculate the field at the focal plane, the two polarization states (*H* and *V*) were independently and numerically propagated to the focal plane using the angular spectrum method to give $C'_{jH}(x, y)$ and $C'_{jV}(x, y)$. The intensity at the focal plane was calculated as $I'(x, y) = C'_{jH}(x, y)^2 + C'_{jV}(x, y)^2$.

In Fig. 7, the results of one run of the simulation of the field in the focal plane from a PM multicore fibre are compared with those of a non-PM multicore fibre with the same geometry. Fig. 7(a) and (e) show the intensity distribution of the horizontal (*H*) polarization state simulated at the distal end of both the PM and non-PM simulated multicore fibres. The separation distance between adjacent cores was set at 21.5 μm and the focal length simulated was 400 μm. Fig. 7(d) and (h) show central line profiles through the intensity and two-photon intensity distributions simulated in the focal plane for both multicore fibres.

In the case of the non-PM multicore fibre, there is a variation in the simulated intensity distribution between successive runs of the MATLAB code due to the background speckle pattern formed by the perpendicular (*V*) component of the field for which the phase is random. By running the simulation 30 times, we found that the PM multicore fibre is expected to provide a 5.13 $\pm$ 0.18-fold (mean $\pm$ standard error in mean) increase in fluorescence signal compared to the non-PM multicore fibre, which is in agreement with the theoretical value calculated above.

IV. Conclusion

We have reported an adaptive multiphoton fluorescence endomicroscope implemented with a double-clad PM multicore fibre for the first time that is demonstrated to generate and scan a focused beam at the distal end with no distal optics or mechanical components. We note that our calculations indicate that the PM multicore fibre provides significantly higher excitation power for multiphoton endoscopic imaging compared to non-PM fibres. In addition, we have demonstrated dynamic correction of the proximal phase distribution at up to 100 Hz update rate, which is a key step towards practical adaptive endoscopes. Currently our imaging rate is determined by the switching rate

of the SLM liquid crystals (approximately 100 Hz) that is used to control the phase tilt on the light emerging from the fibre cores. This imaging rate could be increased by incorporating a galvanometric scanner at the proximal end of the multicore fibre [19], [34] and/or using a liquid crystal SLM with a faster update rate [35]. Thus, we envisage that our adaptive multiphoton endomicroscopy can be developed to provide imaging speeds sufficient for practical preclinical and clinical applications. We note that our experimental and numerical results indicate that the maximum size of object that can be imaged by this adaptive endoscope is limited by the scale of the lattice of foci that are (inevitably) generated by the interference of coherent radiation resulting from the periodic core structure of the multicore optical fibre. In the future the maximum size of object that can be imaged can be increased by designing a multicore fibre with smaller center-to-center separation of cores or by designing a fibre with a less periodic distribution of cores.

ACKNOWLEDGMENT

The authors would like to thank Dr. B. Sherlock for helpful discussions.

REFERENCES

[1] W. Denk, J. H. Strickler, and W. W. Webb, "Two-photon laser scanning fluorescence microscopy," *Science*, vol. 248, pp. 73–76, 1990.
[2] W. R. Zipfel, R. M. Williams, and W. W. Webb, "Nonlinear magic: multiphoton microscopy in the biosciences," *Nature Biotechnol.*, vol. 21, pp. 1369–1377, 2003.
[3] P. T. So, C. Y. Dong, B. R. Masters, and K. M. Berland, "Two-photon excitation fluorescence microscopy," *Annu. Rev. Biomed. Eng.*, vol. 2, pp. 399–429, 2000.
[4] C. Xu, W. Zipfel, J. B. Shear, R. M. Williams, and W. W. Webb, "Multiphoton fluorescence excitation: New spectral windows for biological nonlinear microscopy," *Proc. Nat. Acad. Aci. USA*, vol. 93, pp. 10763–10768, 1996.
[5] D. R. Rivera, C. M. Brown, D. G. Ouzounov, I. Pavlova, D. Kobat, W. W. Webb, and C. Xu, "Compact and flexible raster scanning multiphoton endoscope capable of imaging unstained tissue," *Proc. Nat. Acad. Aci. USA*, vol. 108, pp. 17598–17603, 2011.
[6] F. Helmchen, M. S. Fee, D. W. Tank, and W. Denk, "A miniature head-mounted two-photon microscope: High-resolution brain imaging in freely moving animals," *Neuron*, vol. 31, pp. 903–912, 2001.
[7] M. T. Myaing, D. J. MacDonald, and X. Li, "Fiber-optic scanning two-photon fluorescence endoscope," *Opt. Lett.*, vol. 31, pp. 1076–1078, 2006.
[8] C. J. Engelbrecht, R. S. Johnston, E. J. Seibel, and F. Helmchen, "Ultra-compact fiber-optic two-photon microscope for functional fluorescence imaging in vivo," *Opt. Exp.*, vol. 16, pp. 5556–5564, 2008.
[9] Y. Wu, Y. Leng, J. Xi, and X. Li, "Scanning all-fiber-optic endomicroscopy system for 3D nonlinear optical imaging of biological tissues," *Opt. Exp.*, vol. 17, pp. 7907–7915, 2009.
[10] J. Sawinski and W. Denk, "Miniature random-access fiber scanner for in vivo multiphoton imaging," *J. Appl. Phys.*, vol. 102, 034701, 2007.
[11] R. Le Harzic, M. Weinigel, I. Riemann, K. König, and B. Messerschmidt, "Nonlinear optical endoscope based on a compact two axes piezo scanner and a miniature objective lens," *Opt. Exp.*, vol. 16, pp. 20588–20596, 2008.
[12] L. Fu, A. Jain, C. Cranfield, H. Xie, and M. Gu, "Three-dimensional nonlinear optical endoscopy," *J. Biomed. Opt.*, vol. 12, pp. 040501–040503, 2007.
[13] W. Piyawattanametha, R. P. J. Barretto, T. H. Ko, B. A. Flusberg, E. D. Cocker, H. Ra, D. Lee, O. Solgaard, and M. J. Schnitzer, "Fast-scanning two-photon fluorescence imaging based on a microelectromechanical systems two-dimensional scanning mirror," *Opt. Lett.*, vol. 31, pp. 2018–2020, 2006.
[14] S. Tang, W. Jung, D. McCormick, T. Xie, J. Su, Y.-C. Ahn, B. J. Tromberg, and Z. Chen, "Design and implementation of fiber-based multiphoton endoscopy with microelectromechanical systems scanning," *J. Biomed. Opt.*, vol. 14, pp. 034005–034007, 2009.
[15] L. Fu, A. Jain, H. Xie, C. Cranfield, and M. Gu, "Nonlinear optical endoscopy based on a double-clad photonic crystal fiber and a MEMS mirror," *Opt. Exp.*, vol. 14, pp. 1027–1032, 2006.
[16] C. J. Engelbrecht, R. S. Johnston, E. J. Seibel, and F. Helmchen, "Ultra-compact fiber-optic two-photon microscope for functional fluorescence imaging in vivo," *Opt. Exp.*, vol. 16, pp. 5556–5564, 2008.
[17] E. Laemmel, M. Genet, G. L. Goualher, A. Perchant, J.-F. L. Gargasson, and E. Vicaut, "Fibered confocal fluorescence microscopy (Cell-viZio) facilitates extended imaging in the field of microcirculation. a comparison with intravital microscopy," *J. Vasc. Res.*, vol. 41, pp. 400–411, 2004.
[18] A. J. Thompson, C. Paterson, M. A. Neil, C. Dunsby, and P. M. French, "Adaptive phase compensation for ultracompact laser scanning endomicroscopy," *Opt. Lett.*, vol. 36, pp. 1707–1709, 2011.
[19] E. R. Andresen, G. Bouwmans, S. Monneret, and H. Rigneault, "Two-photon lensless endoscope," *Opt. Exp.*, vol. 21, pp. 20713–20721, 2013.
[20] J. W. Hardy, *Adaptive Optics for Astronomical Telescopes*. London, U.K.: Oxford Univ. Press, 1998.
[21] I. M. Vellekoop and A. P. Mosk, "Focusing coherent light through opaque strongly scattering media," *Opt. Lett.*, vol. 32, pp. 2309–2311, 2007.
[22] O. Katz, E. Small, Y. Bromberg, and Y. Silberberg, "Focusing and compression of ultrashort pulses through scattering media," *Nature Photon.*, vol. 5, pp. 372–377, 2011.
[23] A. P. Mosk, A. Lagendijk, G. Lerosey, and M. Fink, "Controlling waves in space and time for imaging and focusing in complex media," *Nature Photon.*, vol. 6, pp. 283–292, 2012.
[24] T. Čižmár and K. Dholakia, "Exploiting multimode waveguides for pure fibre-based imaging," *Nature Commun.*, vol. 3, art. no. 1027, 2012.
[25] Y. Choi, C. Yoon, M. Kim, T. D. Yang, C. F.-Yen, R. R. Dasari, K. J. Lee, and W. Choi, "Scanner-free and wide-field endoscopic imaging by using a single multimode optical fiber," *Phys. Rev. Lett.*, vol. 109, 203901, 2012.
[26] I. N. Papadopoulos, S. Farahi, C. Moser, and D. Psaltis, "High-resolution, lensless endoscope based on digital scanning through a multimode optical fiber," *Biomed. Opt. Exp.*, vol. 4, pp. 260–270, 2013.
[27] E. E. Morales-Delgado, S. Farahi, I. N. Papadopoulos, D. Psaltis, and C. Moser, "Delivery of focused short pulses through a multimode fiber," *Opt. Exp.*, vol. 23, pp. 9109–9120, 2015.
[28] A. M. Caravaca-Aguirre, E. Niv, D. B. Conkey, and R. Piestun, "Real-time resilient focusing through a bending multimode fiber," *Opt. Exp.*, vol. 21, pp. 12881–12887, 2013.
[29] J. Stone, F. Yu, and J. Knight, "Highly birefringent 98-core fiber," *Opt. Lett.*, vol. 39, pp. 4568–4570, 2014.
[30] A. J. Thompson, "Developing endoscopic instrumentation and techniques for in vivo fluorescence lifetime imaging and spectroscopy," Ph.D. dissertation, Imperial College, London, U.K., 2013.
[31] M. Takeda, H. Ina, and S. Kobayashi, "Fourier-transform method of fringe-pattern analysis for computer-based topography and interferometry," *J. Opt. Soc. Amer.*, vol. 72, pp. 156–160, 1982.
[32] P. K. A. Wai and C. R. Menyuk, "Anisotropic diffusion of the state of polarization in optical fibers with randomly varying birefringence," *Opt. Lett.*, vol. 20 pp. 2493–2495, 1995.
[33] J. W. Goodman, *Introduction to Fourier Optics*. New York, NY, USA: McGraw-Hill, 1996.
[34] E. R. Andresen, G. Bouwmans, S. Monneret, and H. Rigneault, "Toward endoscopes with no distal optics: video-rate scanning microscopy through a fiber bundle," *Opt. Lett.*, vol. 38, pp. 609–611, 2013.
[35] G. Thalhammer, R. W. Bowman, G. D. Love, M. J. Padgett, and M. Ritsch-Marte, "Speeding up liquid crystal SLMs using overdrive with phase change reduction," *Opt. Exp.*, vol. 21, pp. 1779–1797, 2013.

Youngchan Kim was born in Seoul, Korea, in 1981. He received the B.S. degree in physics from Chung-Ang University, Seoul, Korea, in 2006 and the M.S. and Ph.D. degrees for work on terahertz time-domain spectroscopy from Korea Advanced Institute of Science and Technology (KAIST), Daejeon, South Korea, in 2008 and 2011, respectively.

From 2011 to 2013, he worked on quantitative phase imaging as a Postdoctoral Researcher at KAIST. From 2013 to 2015, he was a Postdoctoral Research Associate at the Photonics Group, Imperial College London, U.K. His current research interests include the development and application of novel optical tools to biomedical research.

Sean C. Warren received the M.Sci. degree in physics from the University of Cambridge, London, U.K., in 2008, the M.Res. degree in the chemical biology of disease and health, and the Ph.D. degree from Imperial College London, U.K., in 2010 and 2014, respectively.

From 2014 to 2015, he was a Research Associate in the Photonics group at Imperial College London. His research interests include the application of adaptive optics to biological imaging.

James M. Stone received the M.Phys. and Ph.D. degrees from the University of Bath, Bath, U.K., in 2005 and 2009, respectively.

His research since 2009 has been focused on the design, fabrication, and application of new optical fibers for the study of nonlinear optics and for use in healthcare.

Jonathan C. Knight was born in Lusaka in 1964. He received the undergraduate degree, M.Sc., and Ph.D. degrees from the University of Cape Town, Cape Town, South Africa.

He performed postdoctoral research at the Ecole Normale Superieure in Paris and at the Optoelectronics Research Centre in Southampton. Since 1996, he has worked at the University of Bath, where he has at various times been the Director of the Centre for Photonics and Photonic Materials, the Head of the Department of Physics, and the Associate Dean (Research) for the Faculty of Science. He is currently Pro-Vice Chancellor (Research).

His research interests include linear and nonlinear fiber optics. He is a Fellow of the OSA and received the IOP's Optics and Photonics Prize.

Mark A. A. Neil, photograph and biography not available at the time of publication.

Carl Paterson received the Ph.D. degree in physics from the University of London, London, U.K., in 1996 for work on diffractive optics and optical vortices. He subsequently worked as a postdoctoral Research Associate at Imperial College, London, working on excimer laser ablation for micromachining.

In 2001, he received the Royal Society Research Fellowship to work on adaptive optics. He is currently a Reader in the Physics Department, Imperial College. His earlier research in adaptive optics included its application to compensation of strong atmospheric turbulence for line-of-sight communication and to retinal imaging. Current research interests focus on Brillouin microscopy on the development of adaptive optics techniques for microscopy and endoscopy for in-vivo biological and medical imaging.

Chris W. Dunsby received the M.Sci. degree from Bristol University, Bristol, U.K., in 2000. In 2003, he received the Ph.D. degree from Imperial College, U.K., in "wide-field coherence-gated imaging techniques including photorefractive holography."

He is currently a Reader with a joint post between Photonics, Department of Physics, and the Centre for Histopathology, Department of Medicine at Imperial. His research interests are centered on the application of photonics and ultrafast laser technology to biomedical imaging and include multiphoton microscopy, multiparameter fluorescence imaging, and fluorescence lifetime imaging.

Paul M. W. French received the B.Sc. (Hons.) degree in physics in 1983 and the Ph.D. degree in laser optics from Imperial College, London, U.K., in 1987.

Since 1999, he has been a Professor in the Photonics Group of the Physics Department, Imperial College London, where he was a Royal Society University Research Fellow from 1989 until 1994 when he joined the academic staff, serving as the Head of the Photonics Group from 2001–2013. He has also been a Visiting Professor at the University of New Mexico in 1988 and worked at AT&T Bell Laboratories, Holmdel, NJ, USA in 1990–1991. His research has evolved from ultrafast dye and solid-state laser physics to biomedical optics with a particular emphasis on FLIM for applications in molecular cell biology, drug discovery, and clinical diagnosis. His current portfolio includes the development and application of multidimensional fluorescence imaging technology for microscopy, endoscopy, and tomography.

Prof. French is a Fellow of the Institute of Physics, the European Physical Society, and the Optical Society of America. He received a Royal Society Wolfson Research Merit Award (2007–2012) and the 2013 Joule Medal and Prize of the Institute of Physics.